Facultad de Ciencias
Universidad Zaragoza

Instituto Universitario de Investigación
en Nanociencia de Aragón
Universidad Zaragoza

Final Master Project

Functional nanomaterials based on focused ion irradiation

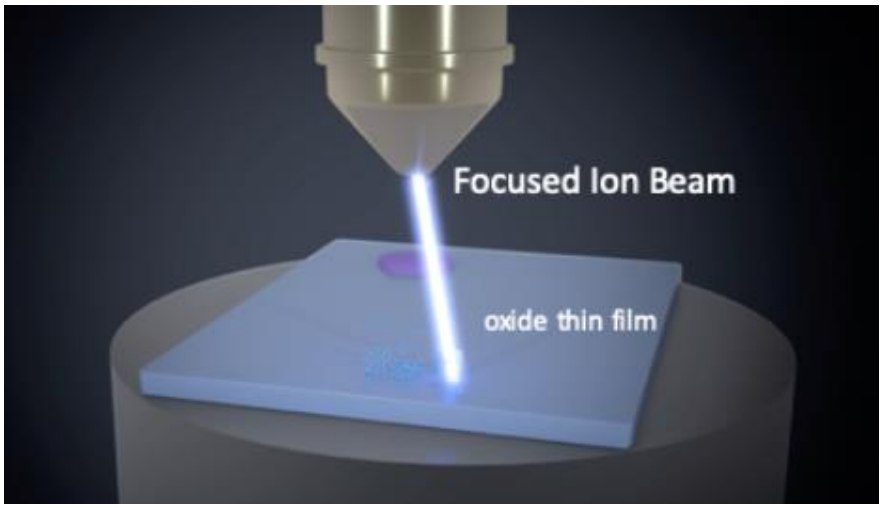

Author:

Alba Hernández Grimal

Supervisors:

Pilar Cea Mingueza

José María De Teresa Nogueras

Master Degree in Nanostructured Materials for Nanotechnology Applications

Facultad de Ciencias / Instituto de Nanociencia de Aragón (INA)

2019 – 2020

Title: Functional nanomaterials based on focused ion irradiation

Author: Alba Hernández Grimal

Supervisors: Pilar Cea Mingueza and José María de Teresa Nogueras

Departments of Physical Chemistry and Condensed Matter Physics

Realization place: Science Faculty and Nanoscience Institute of Aragon

Deposition date: 4 th December 2019

INDEX

Abstract

This final master project aims to study $SrFeO_3$ perovskite, a thin film oxide.

The focused ion beam technique is used to modify the surface of the sample by producing a topotactical transformation in this thin film, which means that in this way, in the transition, the $SrFeO_3$ structure loses oxygen atoms giving rise to the crystallographic transformation Perovskite (PV) - Brownmillerite (BM). These two structures have important differences in electrical properties and wettability properties, which are discussed during the study.

Once the transformation has been induced by different irradiation times, the physical changes with respect to time are analysed by Raman spectroscopy and atomic force microscopy.

1. Introduction

1.1 Nanomaterials and their characterizations

Nowadays, as human needs increase, the development of new materials with advanced properties is growing at the same time. For this reason, knowledge of the properties, characteristics and applications of the material are essential.

It has been demonstrated that the physicochemical properties of any material are the result of its microstructure, that is, the ordered or disordered way in which the atoms that constitute it are located and are directly related to its atomic structure (1) and atomic defects.

Conventional approaches for obtaining new materials with specific properties are based on the use of different chemical compounds and materials by controlling the chemical composition. But in recent years, the promising route for controlling material properties is focused on controlling the size of matter and the particles that make it up, which leads to properties that cannot be produced by conventional systems. (2)

Therefore, progress in the development of techniques (3) in nanosynthesis and nanofabrication used to obtain nanomaterials and nanodevices, in addition to the control of their specific properties (4) , have acquired a very important interest in recent years. In parallel to this development, new tools such as transmission electron microscopy (TEM), scanning probe microscopy systems including scanning transmission microscopy (STM) and atomic force microscopy (AFM), Raman spectroscopy, among other techniques, have allowed us to explore the origin of the physical-chemical properties of these nanoparticles. (2)

Nanomaterials can be synthesized as nanoparticles in solution but also synthesized directly on a support creating a thin film (3). Thin solid films are layers that are in contact with a surface, which acts as a substrate, and with the environment. Their particular thickness compared to their lateral dimensions makes them systems that are infinite in two dimensions and are enclosed between a gaseous phase and a solid phase. As a result, the overall property of a thin film is the combination of mass and interface and the function is identical over the entire film surface. (5)

In particular, thin films of oxides show great interest due to the electronic and magnetic properties of functional oxides (6). There are several techniques capable of synthesizing these films:

- Molecular beam epitaxial (MBE). This technique is able to control the speed of individual cations to perform the epitaxial growth of oxide compounds that are unstable in the bulk, creating atomically precise structures. The disadvantage is that sufficient oxygen needs to be supplied to the film to stabilize the crystal structure.

- Atomic layer deposition (ALD). It is based on two reactions between gas phase precursor molecules and a solid surface. The surface is exposed to a first gas that reacts with the initial surface sites and the reaction stops when all sites are finished. Then, the surface is exposed to a second gas, which reacts with the surface reaction sites from the previous reaction. The advantage of this technique is that the thickness can be controlled only by the number of cycles and it produces very homogeneous films.

- Pulse laser deposition (PLD). This is the most widely used technique for obtaining a wide variety of functional oxides. In PLD, short pulses of ultraviolet light are used to ablate material from a target. The short pulse duration ensures that the generalised heating of the target is low and therefore that thermal evaporation is reduced to a minimum. PLD is a very accurate technique in controlling stoichiometry and epitaxial growth.

In addition, crystalline oxides are compounds with a complex atomic structure, as they can host different types of ions and bonds between them.

This is the case when it refers to transition metal ions (7) with various oxidation states. However, especially mixed transition metal oxides form a series of compounds with a very wide range of electronic properties. They are useful materials in various applications and they are key in the development of nanodevices (1) with enhanced efficiency if they are properly controlled. More specifically, by the use of solid state synthesis or ceramic

method (7), mixed oxides such as perovskites can be prepared with special morphologies such as single crystals or thin layers which is where this work is focused.

1.2 Perovskites

The perovskite structure is one of the most important structure in the area of solid-state science due to its characteristic compositional flexibility. Its electronic structures show properties which range from insulating to metallic, electronically conductive or even superconducting. They also show magnetic properties (8). Some of them are ionic conductive and others have catalytic properties (9).

This abundance of properties makes them excellent candidates for various technological applications: dielectric (10) and piezoelectric components, magnetic memory (11) components and also in solar cells (9) among others.

Perovskites (12) are a family of materials with a common cubic structure, derived from titanium-calcium oxide ($CaTiO_3$). They have a general ABX_3 formula, where A and B are cations of different size, while X is an anion, typically oxygen or halogens. Their structure can be described as BX_6 octahedral joined by their vertices, with cation A occupying the cubo-octahedral gap formed them, as we can see in Figure 1.

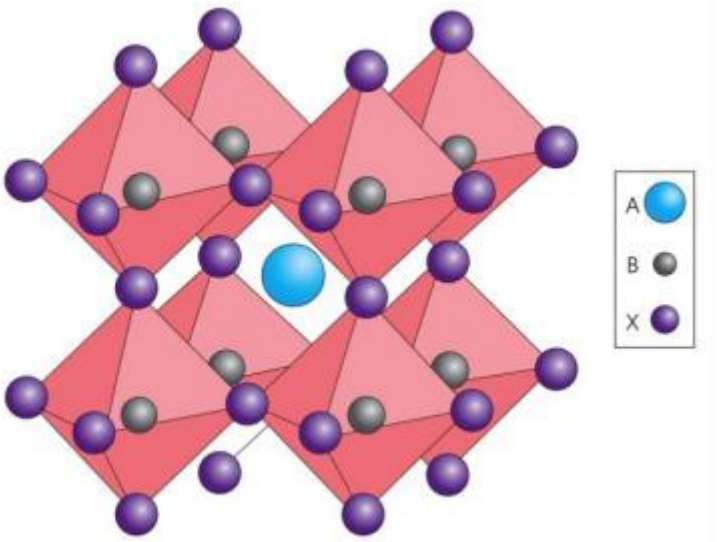

Figure 1. General Perovskite crystal structure. (12)

For example, $MFeO_3$ perovskites (13) are able to have different properties depending on the type of metal and its lattice parameter. In particular, $LaFeO_3$ is an antiferromagnetic insulator, $SrFeO_3$ is a metal and $CaFeO_3$ is a semiconductor system. Furthermore, the properties of $MFeO_3$ phases can change radically depending on factors such as stoichiometry (the presence of oxygen vacancies in the lattice), temperature and external pressure.

1.3 $SrFeO_x$ system

The stroncium ferrite $SrFeO_x$ (SFO) system (14) is a system that has different physical and chemical properties that can be modified as a function of temperature and magnetic field. The structure of $SrFeO_x$ changes depending on the oxygen content and the vacancies in the lattice.

$SrFeO_x$ forms a cubic structure (Figure 1) with the composition $SrFeO_3$ with Fe (IV) and an orthorhombic structure in $SrFeO_{2.5}$, where there is Fe (III). The last complex has a brownmillerite (14) type structure, as shown in Figure 2, which results in an oxygen-deficient perovskite consisting of alternating octahedral layers typical of FeO_6 octahedral perovskite sharing vertices with tetrahedral FeO_4 layers.

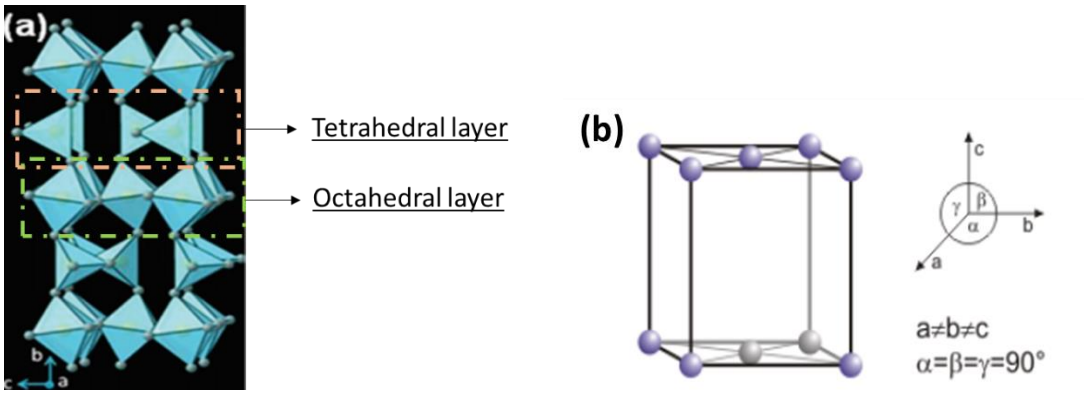

Figure 2. (a) Brownmillerite structure (14) with tetrahedral and octahedral layers. (b) Orthorhombic system.

Among all the iron oxides, the cubic perovskite $SrFeO_3$ is one of the most interesting for the study of the effects of oxygen deficiency in terms of electronic and structural properties. (15) Therefore this can be summarized in the existence of a $SrFeO_{3-\delta}$ system.

The compound $SrFeO_{3-\delta}$ is a complex oxide that allows the variation of stechiometric oxygen between $0 \leqslant x \leqslant 1$. In particular the reversible transformation is observed for $0 \leqslant x \leqslant 0.5$, because the $SrFeO_2$ (16) Fe (II) structure can only be obtained by a low temperature reduction using CaH_2 resulting in an infinite layer structure with a planar-square coordination of the metal. In between the transformation are the intermediates $SrFeO_{2.875}$ and $SrFeO_{2.75}$ with diffuse streaks which are originated from a modified twin structure transition and the associated changes in the domain structure developed during the oxygen intercalation (17). Finally, the transformation results in a stable $SrFeO_{2.5}$ structure showing a tetrahedral stacking along the stacking axis of the brownmillerite unit cell.

In summary, the $SrFeO_{3-\delta}$ (SFO) perovskite thin films have a large range of physical properties that have great interest from the scientific and nanotechnological field, because of the different valence states of Fe, which allows for various stable states of oxygen occupancy in the lattice.

So much so, that $SrFeO_{2.5}$ shows a semiconductor behaviour and a brownmillerite (18) structure, while $SrFeO_3$ shows a metallic behaviour with a helical magnetic structural order.

Therefore the interest is in the change from $SrFeO_3$ (PV) to $SrFeO_{2.5}$ (BM) where this oxygen variation causes a crystallographic transformation which is called a topotactic transformation.

1.4 Topotactic transformation PV-BM

Oxygen stoichiometry plays the most important role in determining the crystal structure and physical properties of transition metal oxides.

As a result, by means of a chemical redox reaction the oxygen content can be altered and the functionality of these oxides can be changed. A phase transformation called topotactic takes place, which is associated with the insertion/release of a quantity of oxygen ions into the structure without breaking the lattice. (19)

By definition, they are transformations of the crystalline structure by means of a solid-state reaction.

In particular, this topotactical phase transformation facilitates the redox process in perovskites with oxygen vacancy arrangement by varying the concentration of a material without losing the network structure as shown in Figure 3.

$SrFeO_3$ presents all of the iron ions at the octahedral interstices surrounded by six oxygen atoms, by extracting one out of six oxygen atoms contained in the lattice of the strontium ferrate (IV). However, in the structure of the strontium ferrate (III), alternate octahedral and tetrahedral coordination of the iron ions are arranged in chains parallel to the axis of its orthorhombic cell.

Both structures have different crystal symmetries, orthorhombic and cubic, but from the crystallographic point of view, the brownmillerite structure is referred to as an ordered oxygen deficient perovskite structure.

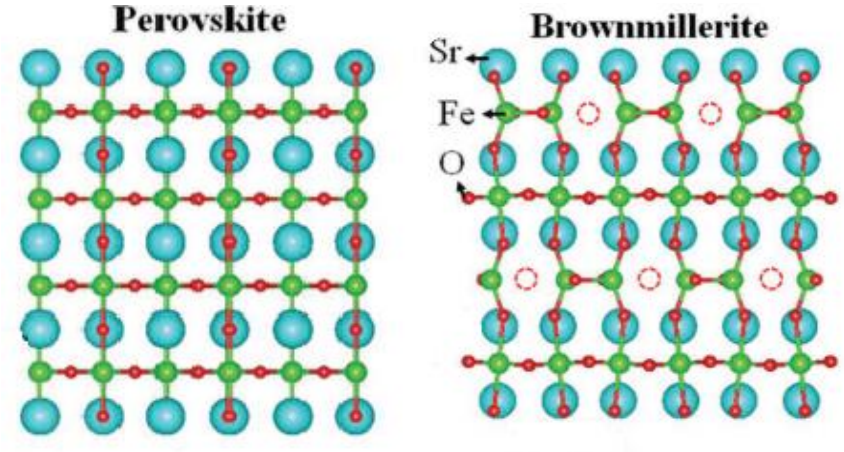

Figure 3. Schemes of lattice structures PV and BM, taken and adapted from reference (19).

As mentioned above, $SrFeO_x$ ($2.5 \leqslant x \leqslant 3$) is considered to be a very suitable system for the study of the topotactic phase transformation induced by a reversible redox reaction. And in comparison with other multivalent transition metal oxides that exhibit a topotactical transformation, the Earth's abundant nature, low cost and non-toxic nature of Fe provides a major attraction to $SrFeO_x$. (20)

$SrFeO_{3-x}$ is unique in that its exhibits a wide range of oxygen deficiency and crystallizes as a cubic perovskite when the material is prepared in the normal solid state reaction.

A study confirmed that the transformation of the PV-BM topotactic phase depends on environmental pressure and temperature. The PV thin film was placed in vacuum ($P=10^{-7}$ Torr) and the temperature was increased to release oxygen. After the transformation, the sample was cooled without breaking the vacuum and this BM phase was thermodynamically adapted to the ambient temperature. To give the reversible process from BM to PV phase it was done in an oxidizing environment. (20)

On the other hand, the PV-BM topotactic transformation of $SrFeO_x$ ($2.5 \leqslant x \leqslant 3$) thin films can be induced locally with submicrometer spatial resolution at room temperature by an electric field created by an AFM-tip (Figure 4). This work offered a new approach to transformation since the crystallographic transformation was achieved at room temperature and the process was carried out under ambient conditions without the need to modify the film surface. (21)

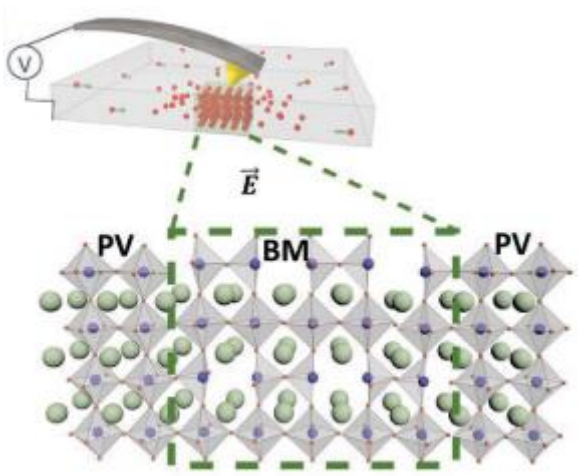

Figure 4. AFM electric-field-induced local topotactic transformation, taken from reference (21).

As a conclusion, this phase transition is a change in physical properties, including electronic transport, magnetic properties and in electronic structures. Therefore, by means of an epitaxial synthesis and by controlling the electrochemical and catalytic effects of the surface, two topotactic phase films with evident differences in oxygen concentration and different valence states can be obtained, offering the opportunity to develop high performance perovskite-based oxide ionic devices. Moreover, nanolithography techniques are expected to produce this transformation locally, with nanoscale dimensions.

2. Hypothesis and Objectives

This work is based on the hypothesis that Ga^{+}-FIB irradiation could induce a topotactic transformation on $SrFeO_{3-\delta}$ thin films, from perovskite crystallographic structure into the brownmillerite (BM). This transformation is expected to result in a structural change that is reflected on a change in the electrical properties and wettability properties of the material under study. Therefore, I have studied such transformation by using different characterization techniques such as atomic force microscopies (AFM) and Raman Spectroscopies.

The mains objectives of the work are:

Academic Objectives

- To work in the nanotechnology field by developing skills in the laboratory, studying new materials with advanced properties and to know their applications as nanodevices.
- Improvement in scientific communication by writing a report about the work carried out and applying knowledge in the interpretation of the experimental results.
- To learn how to perform a rigorous bibliographic research.
- To learn the handling of experimental techniques such as focused ion beam (FIB), atomic force microscopy and Raman spectroscopy.

Scientific objectives

- To investigate the topotactic transition in the same material but grown on different substrates in order to study the change in the electrical properties.
- To investigate the change of wettability properties (hydrophobicity) after the topotactic transition.
- To characterize the transition by means of different experimental techniques such as FIB, atomic force microscopy and Raman spectroscopy.

3. Experimental section

3.1 Sample growth

The sample used during the whole experiment was $SrFeO_3$ on a MgO substrate. These samples were grown in the Professor Francisco Rivadulla´s research group (USC, Santiago de Compostela).

Since the electrical properties of perovskites-based structures largely depend on oxygen content, one way to control this parameter during the film deposition process is to use the PLD technique. This is the reason why this methodology is used for the growth of the studied samples.

The PLD technique was used to grow this epitaxial $SrFeO_3$ thin film structure on the substrate, due to the high dependence that exists in the crystalline-magnetic structure and electrical properties on the oxygen content.

Pulsed laser deposition (22) is a widely used method for the growth of thin films. High energy laser pulses are focused on a target material and are absorbed by the material creating an electronic excitation. This energy is rapidly converted to other forms, including kinetic energy and heat, resulting in laser ablation that releases a plume of ionized particles. By controlling the geometry (Figure 5) of the laser beam and the target material, it is possible to direct the path of the plume, creating a thin film on the surface of the desired substrate. During the growth of the film, both, the target and the substrate are kept in a vacuum. This implies that the ejected material does not interact with the air, avoiding the dispersion of the plume and the deposition of unwanted species on the substrate.

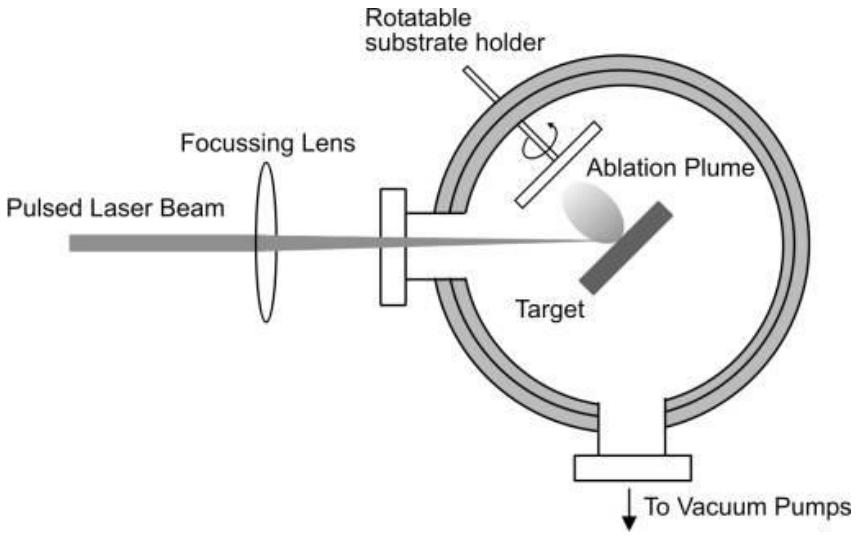

Figure 5. Diagram of the pulsed laser deposition set up.

In particular, PLD is a very useful technique for creating thin films of oxides because the growths are done in a sealed chamber and it is a simple procedure to introduce a background gas during the growth. Varying the oxygen background gas pressure provides a level of control over the oxygen content of the resulting film.

The thin film of $SrFeO_{3-\delta}$ was deposited on single-crystal substrate of MgO from a dense ceramic target by Pulsed Laser Deposition (PLD) (Nd:YAG Laser, lambda=266 nm, 5 Hz, fluence 1.5 J/cm^2) at a temperature of 700ºC, and oxygen pressure of $P(O_2)$=10 mTorr. After deposition the sample was annealed at the growth temperature for 10 min al $P(O_2)$=300 mTorr to obtain the PV. The sample were then rapidly cooled down to room temperature inside the PLD chamber under the same oxygen pressure, to keep the oxygen content.

3.2 Focused ion beam

Focused ion beam (FIB) is a nano-patterning technique that uses an instrument that is almost identical to a scanning electron microscope (SEM), but uses a beam of ions instead of a beam of electrons. The focused ion beam can directly modify the thin film surface, via the sputtering process, and this milling can be controlled with nanometer precision. By carefully controlling the energy and intensity of the ion beam, it is possible to remove the desired material.

Typically, the beam of heavy atoms of Ga^+ is used to bombard a target material. The Ga^+ ions are generated by a liquid metal ion source (LMIS), which is a small reservoir connected to a tungsten needle. When the reservoir is heated, Ga flows to the tip of the needle, forming a small point source. Then, applying a strong electric field to the needle tip, it extracts ions from this source. (23)

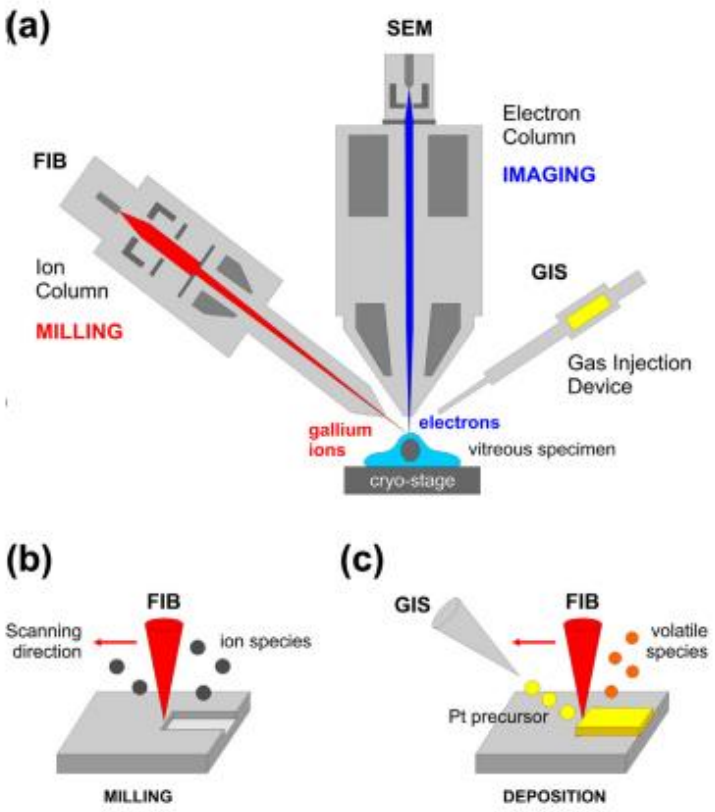

Figure 6. (a) Principle of a FIB-SEM microscope, (b) Ion beam milling to remove material and (c) ion beam deposition to deposit molecules onto the surface: adapted from reference (24).

As we can see in Figure 6, during FIB milling a beam of focused ions are able to remove material from the specimen surface. Blending a FIB instrument with a SEM, makes it possible to simultaneously control the milling procedure with the electron beam and, more importantly, to obtain images of the specimen's surface in a non-destructive manner. Also, a specific one-site material release with an FIB system is achieved by accelerating and focusing a beam of ionised gallium atoms on the surface of the specimen.

The FIB-SEM used in this work was a Dual Beam Helios 600 model that consists of a 30 kV field-emission scanning electron column and a 30 kV Ga^+ Focused Ion Beam placed at 52º one from each other.

3.3 Atomic Force Microscopies

The atomic force microscopy (AFM) is a scanning probe microscope with nanometer scale resolution. It uses a cantilever with a sharp probe that scans the surface of the specimen and when the tip of the probe travels near to a surface, the forces between the tip and sample deflect the cantilever according to Hooke´s law.

The cantilever has a resonant frequency, f_0 and a constant, k that corresponds with the constant in the Hooke´s law (*Equation 1)*. So, according with this equation, depending on the k of the cantilever, we know if it is hard or soft cantilever and over which material it can be used.

$$F = - k \cdot x \quad \text{(Equation 1)}$$

When the tip is close to the sample, interactions are detected by monitoring the reflection of a laser off the cantilever with a photodiode divided in four regions. This optical geometry of the photodiode amplifies the signal and yields a detection limit on the order of 0.1 Å.

In the AFM, a piezoelectric system controls the position of the sample and moves it relative to the tip in the x-y plane for imaging or in the z direction for force measurements.

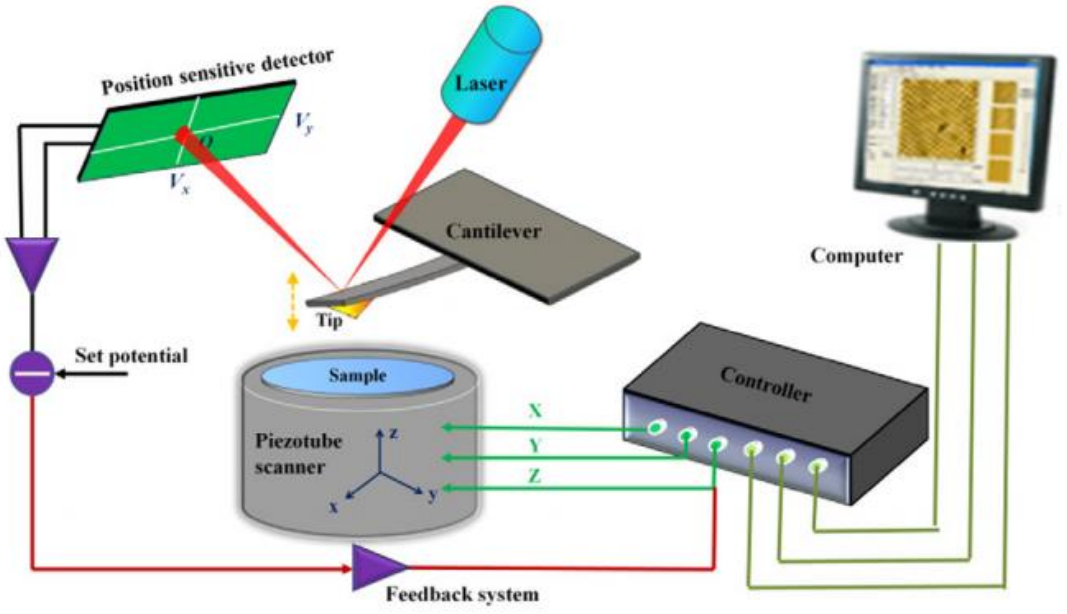

Figure 7. Schematic diagram of the basic working principle of AFM.

Atomic force microscopy (25) was used before to study the chemical differences in the irradiated areas with respect to the non-irradiated area. In this work, the AFM is used to determine the difference in height between the irradiated and non-irradiated areas in the samples, i.e. the change in thickness caused by the FIB irradiation and to determine the differences in the roughness depending on the irradiation conditions.

The equipment used was AFM multimode 8 (Bruker). Tips of the RTESPA – 150 model were used during the experiments.

The experiments were carried out on a nominal resonance frequency of 150 KHz, the nominal spring constant was 5 N/m and the scan rate used was between 0.5 Hz and 1 Hz.

3.4 Raman Spectroscopy

Raman spectroscopy (26) is a high resolution optical technique that provides chemical and structural information of many materials in a short time. It is based on the use of a monochromatic beam light which comes into the sample. A small fraction of that light is inelastically scattered while undergoing small frequency changes that are characteristic of the material analysed.

Analysis by Raman spectroscopy is based on having a beam of monochromatic frequency light incident on a sample whose molecular characteristics are to be determined, and

examining the light scattered by that sample. Most of the scattered light has the same frequency as the incident light but a small fraction has a change in frequency, resulting from the interaction of light with matter. The light that maintains the same frequency v as the incident light is known as Rayleigh scattering and does not provide any information about the composition of the analysed sample. Scattered light with different frequencies from the incident radiation can provide information about the composition of the sample, the lattice structure or the sample's thickness and the technique is known as Raman scattering. These new frequencies are the Raman frequencies, which are characteristic of the chemical nature and physical state of the sample and independent of the incident radiation.

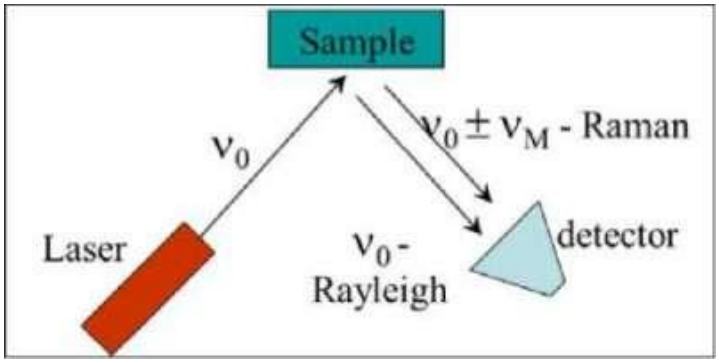

Figure 9. Basic principle of Raman Spectroscopy.

Scattering is the deflection of the light from its original direction of incidence. The interaction of the electric field vector of the electromagnetic wave with the electrons of the system with which it interacts, gives rise to scattering of light, and there are two basic types of scattering: Elastic (same frequency as incident light, also called Rayleigh scattering) and inelastic.

It is the inelastically scattered light that is called Raman scattering and there are two classes. In one of them, the scattered light has lower energy than the incident light and the effect is called Raman Stokes scattering. In the other, the scattered light has higher energy than the incident light, that is, it has a higher frequency than the incident light and it is called anti-Stokes Raman scattering. In contrast, in Rayleigh scattering there is no change in the energy of the incident light. All main vibration modes are reflected in Figure 10.

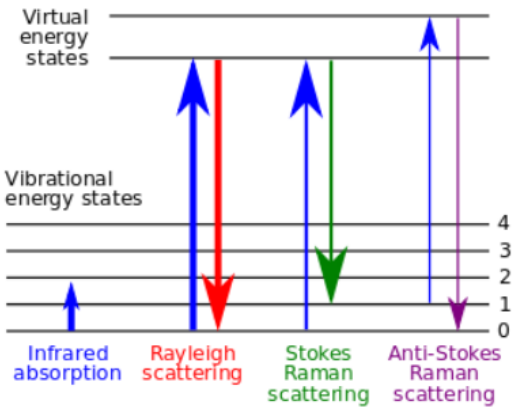

Figure 10. Vibration modes.

The equipment used was a Confocal Raman from Witec, model Alpha300M+.

4. Results and discussion

In this work, the underlying idea is the effect of FIB irradiation to remove oxygen atoms selectively from the original perovskite $SrFeO_3$ film (SFO), triggering the transformation of the irradiated areas into the brownmillerite $SrFeO_{2.5}$ phases, theoretically, producing an expansion of the unit cell, as we can see in Figure 11 .

This crystallographic transformation (21) takes place by removal of oxide-ion positions, without rearrangement of the cations. It can be made reversible by exposure of the BM in air or oxygen at moderate temperature.

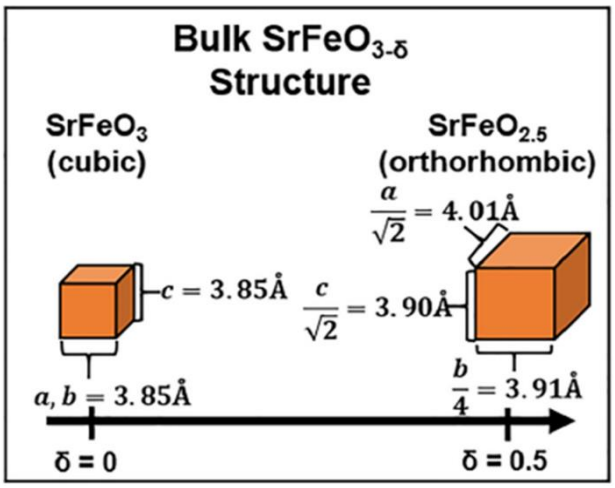

Figure 11. Increase of unit cell parameters.

The expected volume increase in the transition, taking into account the theoretical network parameters in both phases, is approximately 4 $Å^3$. This increase of lattice parameter of SFO films is directly related with the increase of the oxygen vacancies. Then, in an oxygen-rich growth environment, the growth of $SrFeO_3$ is more favoured rather than $SrFeO_{2.5}$ phase. (18)

Then, as mentioned above, the present work uses Ga^+-FIB irradiation to produce this topotactic transformation. Figure 12 shows a TEM image of an unirradiated PV film compared with an irradiated zone.

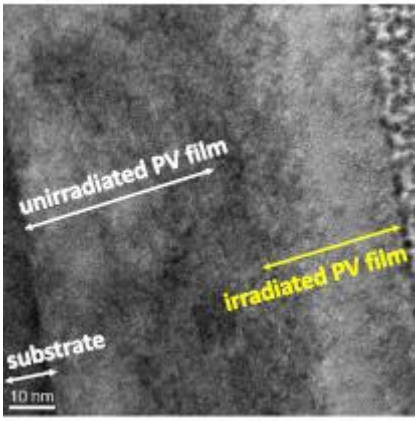

Figure 12. High-resolution cross-sectional TEM image of an unirradiated PV film compared with an irradiated zone. (27)

We assume that Ga^{+}-FIB irradiation can induce a topotactic transformation in $SrFeO_3$ thin films due to the ability of this methodology to remove oxygen atoms selectively from the original film perovskite resulting in a crystallographic transformation in the irradiated areas towards a BM phase. This is mostly a physical effect.

As ion irradiation removes a significant amount of oxygen atoms by preferential sputtering, the perovskite film decreases its energy through its transformation into BM, which is the most stable phase when the oxygen vacancy concentration is large enough.

The approach followed consists of a one-step lithography process. In addition, this procedure does not require resists, allows high-resolution nanopatterning and can be extended to large area substrates if the ion dose required to induce the topotactic transformation is low.

It is well known that the used instrument exhibits the best resolution (4.5 nm) when a 30 kV ion acceleration is applied, due to the minimization of the lens aberrations (27). Under 30 kV, the Ga^{+}-FIB column maximum resolution is 4.5 nm.

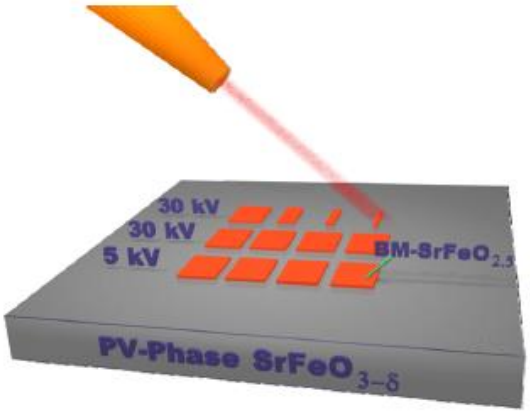

Figure 13. Scheme of the experiment done in this project. Under Ga^+-FIB irradiation, the $SrFeO_{3-\delta}$ film, originally in the PV phase, is transformed into the $SrFeO_{2.5}$ BM phase.

Using 30 kV and low current of 16.6 pA, several areas of initial PV were irradiated by varying the ion dose of Ga^+ at 30 kV (Figure 14). Under 30 kV, the minimum and maximum ion irradiation times used in the experiments were 0.2 and 100 seconds, corresponding to irradiation doses of 12.25 $\mu C/cm^2$ and 6125 $\mu C/cm^2$, respectively.

In Figure 14, there are two areas of the initial perovskite with different rectangles, which correspond to the areas which have been irradiated. The irradiation time (in seconds) for each area is written below the corresponding rectangle. Thus, it is possible to study the differences in properties and physical changes with respect to the irradiation time.

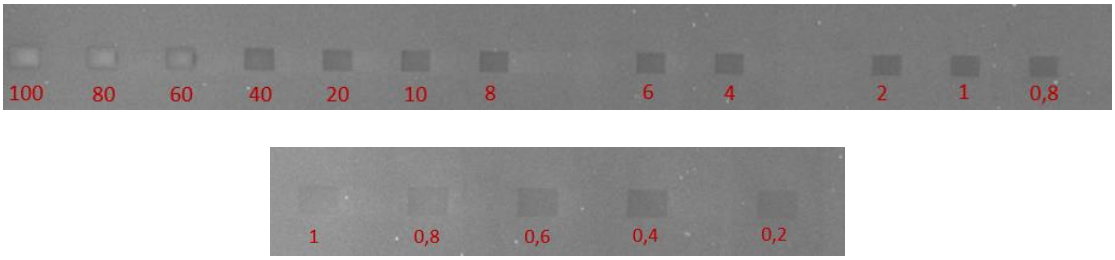

Figure 14. SEM image of PV $SrFeO_{3-\delta}$ thin film after several rectangles (4 x 6 μm^2) were patterned with a Ga^+-FIB irradiation at different doses (time in seconds) using 30 kV ion acceleration.

In the SEM micrograph of Figure 15, the MgO substrate can be seen at the bottom, the initial perovskite in second place with an approximate thickness of 45 nm and then two layers deposited: the first is platinum grown with electrons and the second deposition is platinum grown with ions, in order to determine the milling rate and the layer thickness.

An irradiation time of 500 seconds (Figure 15) under 30 kV and 16.6 pA results in a milling rate of 0.1 nm/s. This means that the film thickness is expecting to decrease ≈ 1 nm after 10 seconds. In addition, the layer thickness is close to 50 nm.

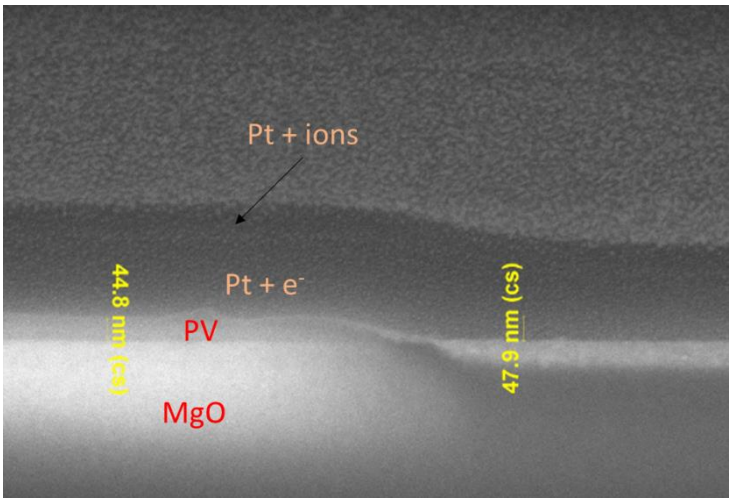

Figure 15. SEM image of a cross section after 500 s of 30 kV Ga irradiation to determine the milling rate.

AFM was used to obtain topographic images of the patterns done by applying different irradiation doses. These images provide information about the homogeneity, height and roughness of the patterned regions here studied.

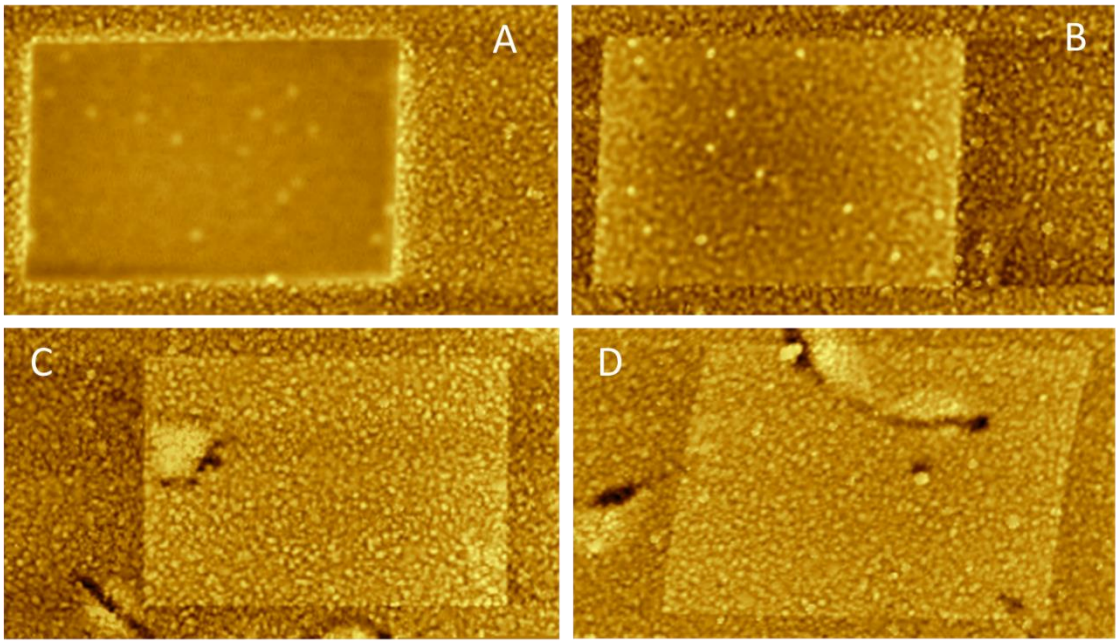

Figure 16. AFM images corresponding to a) 100 seconds, b) 10 seconds, c) 1 second and d) 0.4 seconds irradiation time.

The images were analysed using the Gwyddion software. In addition, the same flattening procedure was applied to all the images.

RMS is the root mean average of the profile height deviations from the mean line. RMS is calculated as the Root Mean Square of the surfaces measured microscopic peaks and valleys (*Equation 2*).

Equation 2. $RMS = \left[\left(\frac{1}{L}\right) \cdot \int_0^L Z(x)^2 \, dx\right]^{1/2}$; where L is the evaluation length and Z(x) is the profile height function.

First, the RMS (Root Mean Squared) roughness of a non-irradiated region was determined. This RMS roughness (≈ 2 nm), corresponds to the pristine perovskite film. Then, taking into account that the roughness of the initial PV perovskite is different from the roughness of the irradiated zones, it can be concluded that there is a structural change and therefore that there are two differentiated phases.

In addition, AFM topography reveals a substantial increase in the film thickness on the irradiated areas. The height (*h*) of the irradiated zone was determined with respect to the

perovskite background by doing profiles in each irradiation area. Figure 17 shows one of the images treated following this procedure and the corresponding profile (Figure 18).

In Figure 17, RMS corresponds to the roughness of the irradiated zone, RMSp corresponds to the roughness of the non-irradiated perovskite, the red line indicates where the profile is made to determine the difference in height between the irradiated and non-irradiated zone, i.e. what is indicated as h. On the right of the image, the colour scale appears to visualise the different heights.

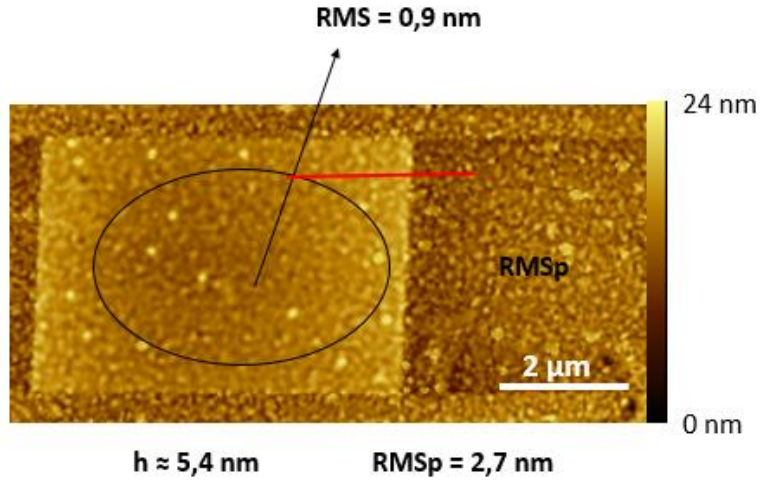

Figure 17. AFM image of the PV after irradiation (squared area) irradiated area for 10 seconds.

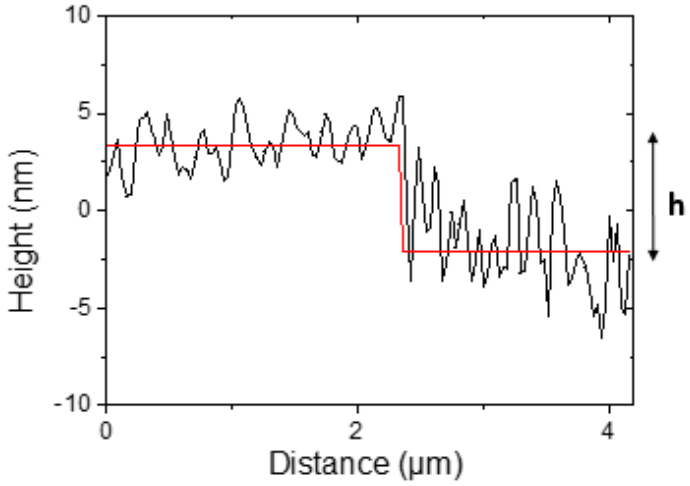

Figure 18. Height profile of the irradiated area for 10 seconds. It corresponds to the red line drawn in Figure 14.

Following this procedure for all irradiated areas, one can observe that there is a significant film thickness increase between 0 s and 20 s, but a thickness decrease between 20 s and 100 s. This result is indicative of an expansion of the unit cell as the irradiation time increases leading to a structural transformation on the thin film, which is in agreement with our hypothesis of a transformation from PV to BM.

In addition to this transformation, the ion irradiation also results in a milling of the film, which explains the decrease in the thin film thickness under high irradiation doses. In the case of 30 kV Ga^+ irradiation, the thickness decreases by more than 6 nm between 20 s and 100 s irradiation times, as we can see in Figure 19.

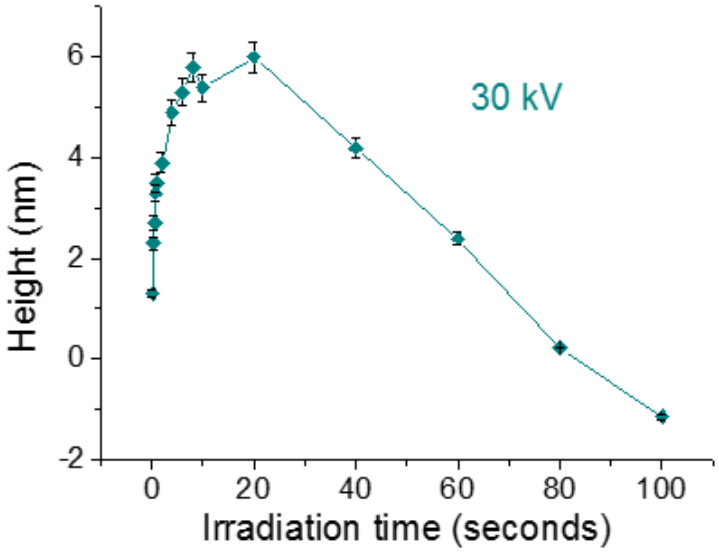

Figure 19. Surface expansion as a function of the irradiation time.

The decrease of heights at high irradiation times is due to the milling effect. At low irradiation times the height increase effect is more important due to the change to the BM phase. Then by adjusting the last 5 points to a straight line, the milling thickness per unit of time can be determined.

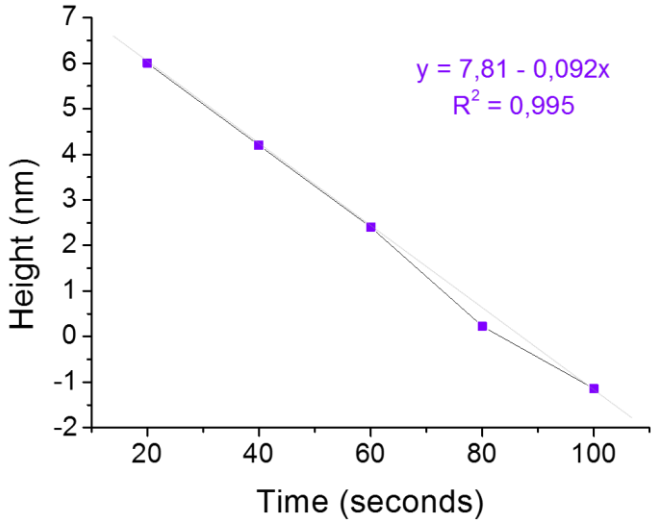

Figure 20. Adjustment of the highest irradiation times with respect to the height difference to obtain the milling thickness

The slope of the line determines the thickness value of the milling. That is, the experimental thickness is 0.092 nm/s. It is close to the milling rate determined in the previous calibration experiment, 0.1 nm/s.

In addition, the roughness increases with decreasing irradiation time and remains nearly constant at high irradiation time as illustrated in Figure 21.

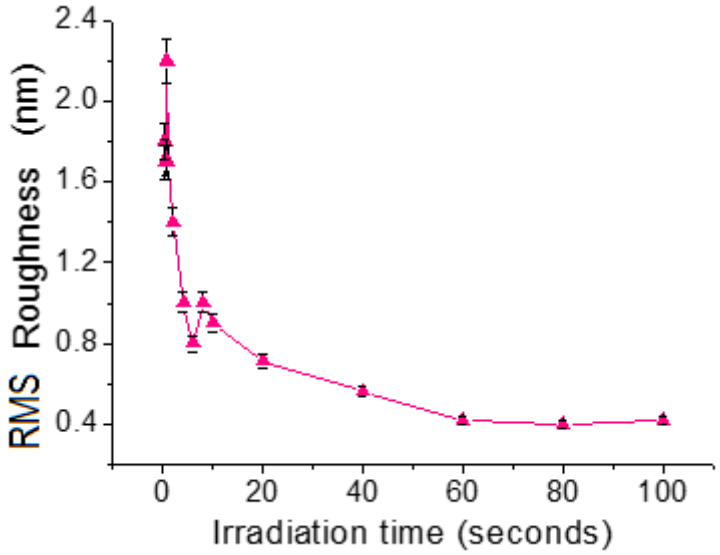

Figure 21. RMS roughness as a function of the irradiation time.

These same irradiated areas were studied with Raman Spectroscopy to determine structural differences in the irradiated areas with respect to the non-irradiated area.

The irradiated areas were also analysed by Raman spectroscopy and compared with the non-irradiated area. Figure 22 shows the change of the signal as a function of the irradiation doses. The peaks appearing around 220 cm^{-1}, 340 cm^{-1}, 440 cm^{-1}, but especially the peak near to 620 cm^{-1} in the non-irradiated region (0 s) are characteristic of the PV phase. As the irradiation time increases, these peaks disappear and a wide band appears above 700 cm^{-1}. This peak is characteristic of the BM phase (28).

Therefore, these results confirm that by Ga^{+}-FIB the transformation from PV phase to the BM phase can be provoked.

On the other hand, the Raman spectra of the areas irradiated at the highest doses show a decrease in the intensity and a widening of the BM peak, suggesting the grinding and amortization of the crystalline structure, a result that is consistent with the data obtained in the AFM.

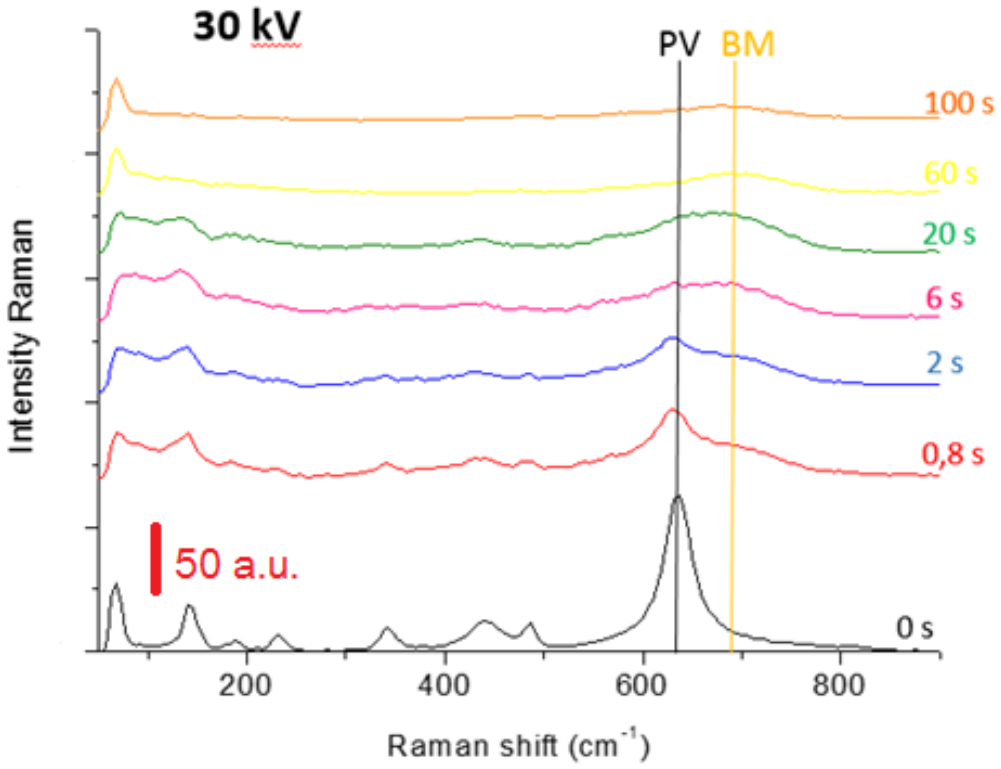

Figure 22. Room-temperature Raman spectra of irradiated areas (λ=532 nm) at 1 mW for the indicated irradiation times compared with the pristine PV sample indicated as 0 s on the bottom of the graph.

Once the irradiations were made at different times and to be able to deduce by means of AFM and Raman that there is evidence of structural changes and therefore to affirm the crystallographic transformation PV-BM, the idea was to make electrical measurements of the initial phase without irradiation and after all the irradiated zones to be able to determine the electrical properties of these oxide thin film. The result was that the sample did not prove to be as good an electrical conductor as initially thought. The initial state was already quite resistive

In addition, we wanted to study through contact angle experiments, the hydrophobicity of oxide film and investigate changes as a function of irradiation doses.

When a drop of water was deposited on the initial perovskite surface, the contact angle changed over time, that is, in a way that we have not studied, the water was reacting with the sample surface and was damaging it, as shown in Figure 23, where the spot that formed on the surface can be seen. These drops were not washing off with any compound.

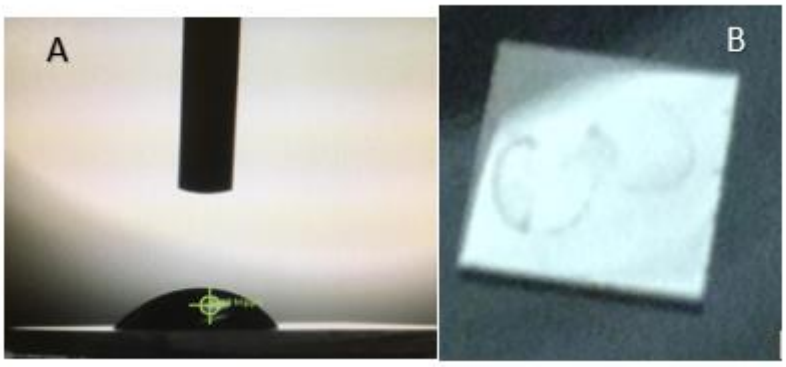

Figure 23. A) Contact angle measurement. B) Surface of the initial perovskite after depositing a drop of water.

To conclude, all experimental measurements have been made of the PV on an MgO substrate. It would be interesting to do all the work on a different substrate, such as $SrTiO_3$ (STO) and thus be able to compare with respect to the substrates as well.

5. Conclusions

The material investigated during this project was $SrFeO_3$ perovskite on an MgO substrate. By means of Ga^+-FIB a crystallographic transformation is induced, removing oxygen atoms selectively and leading to a new structure called brownmillerite $SrFeO_{2.5}$.
The structural changes originated by irradiation shower have been studied by AFM and Raman.

AFM images reveal a substantial expansion of the film thickness of the irradiated areas. Raman spectra are indicative of structural changes due to a change in chemical composition. In other words, focused ion beam may induce phase changes over nanometric regions of controlled area and shape resulting in various structures with different properties within a small region.

To the best of our knowledge, this is the first time that the effect of gallium irradiation on $SrFeO_3$ grown on MgO has been explored. A similar phenomenon had previously been observed on a $LaAlO_3$ substrate. Also, it is the first time that a decrease in roughness has been observed by increasing the irradiation time.

REFERENCES

1. Acharya SK, Dash U, Baik H. Brownmillerite Thin Film as a Fast Ion Conductor for the High- Performance Resistance Switching Memory. *Nanoscale*. **2017**, 9, 10502-10510.

2. Fuchs H, Webster TJ, Tang Z, Banhart F. Functional nanomaterials and their applications: From origins to unanswered questions. *ChemPhysChem*. **2012**, 13(10), 2423–2425.

3. Kumar N, Kumbhat S. Essentials in Nanoscience and Nanotechnology, First Edition, Chapter 2, **2016**, 29–76.

4. Christian P. Environmental and Human Health Impacts of Nanotechnology, Chapter 2, **2009**, 31–77 .

5. Grosso D, Boissière C, Faustini M. Thin Film Deposition Techniques. The Sol-Gel Handbook-Synthesis, Characterization, and Applications. **2015**, 277–316.

6. Blamire MG, MacManus-Driscoll JL, Mathur ND, Barber ZH. The materials science of functional oxide thin films. *Adv Mater.* **2009**, 21, 3827–3839.

7. Amparo L, Santos P. Métodos de síntesis de nuevos materiales basados en metales de transición Synthesis methods of new transition metal materials. *Revista Facultad de Ingeniería* N.˚ 32, **2004**, 51–61.

8. Sa RD, Carbonio RE, Franco DG, Fuertes VC, Blanco MC, Ferna MT. Synthesis, structure and magnetic properties of $La_3Co_2SbO_9$: A double perovskite with competing antiferromagnetic and ferromagnetic interactions. *Journal of Solid State Chemistry*. **2012**, 194, 385–391.

9. Vasala S, Karppinen M. $A_2B'B''O_6$ perovskites: A review. *Progress in Solid State Chemistry*. **2015,** 43(1–2), 1–36.

10. Jain P, Dalal NS, Toby BH, Kroto HW, Cheetham AK. Order - Disorder Antiferroelectric Phase Transition in a Hybrid Inorganic - Organic Framework with the Perovskite Architecture. *J. Am. Chem. Soc*. **2008**, 130, 10450 –10451.

11. Acharya SK, Nallagatla RV, Togibasa O, Lee BW, Liu C, Jung CU, et al. Epitaxial

Brownmillerite Oxide Thin Films for Reliable Switching Memory. *ACS Appl. Mater. Interfaces*. **2016,** 8, 7902-7911**.**

12. Green MA, Ho-Baillie A, Snaith HJ. The emergence of perovskite solar cells. *Nat Photonics*. **2014**, 8(7), 506-514.

13. Shein IR, Shein KI, Kozhevnikov VL, Ivanovskiĭ AL. Band structure and the magnetic and elastic properties of $SrFeO_3$ and $LaFeO_3$ perovskites. *Phys Solid State*. **2005**, 47(11), 2082–2088.

14. Suchita KB, Singh S. Synthesis and characterization of brownmillerite $SrFeO_{2.5}$ in nanostructured form. *Solid State Physics*. **2015**, 1665.

15. Takano M, Okita T, Nakayama N, Takeda Y. Dependence of the Structure on Composition and Electronic State of SrFeO , and Temperature. *Journal of Solid State Chemistry*. **1988**, 73(1), 140-150.

16. Tsujimoto Y, Tassel C, Hayashi N, Watanabe T, Kageyama H, Yoshimura K, et al. Infinite-layer iron oxide with a square-planar coordination. *Nature.* **2007**, 450, 1062-1065.

17. Maity A, Dutta R, Penkala B, Ceretti M. Solid-state reactivity explored in situ by synchrotron radiation on single crystals : From $SrFeO_2$ to $SrFeO_3$ via electrochemical oxygen intercalation. *Journal of Physics D Applied Physics.* **2015**, 48(50), 504004.

18. Enriquez E, Chen A, Harrell Z, Lü X, Dowden P, Koskelo N, et al. Oxygen vacancy-driven evolution of structural and electrical properties in $SrFeO_{3-\delta}$ thin films and a method of stabilization. *Appl Phys Lett*. **2016**, 109(14), 3–8.

19. Tian J, Wu H, Fan Z, Zhang Y, Pennycook SJ, Zheng D, et al. Nanoscale Topotactic Phase Transformation in SrFeOx Epitaxial Thin Films for High-Density Resistive Switching Memory. *Adv Mater*. **2019,** 31, 1903679.

20. Khare A, Shin D, Yoo TS, Kim M, Kang TD, Lee J, et al. Topotactic Metal – Insulator Transition in Epitaxial $SrFeO_x$ Thin Films. *Adv Mate*r, **2017**, 29, 1606566.

21. Ferreiro-vila E, Blanco-canosa S, Lucas I, Vasili HB, Magén C, Ibarra A, et al. Room-Temperature AFM Electric-Field-Induced Topotactic Transformation

between Perovskite and Brownmillerite $SrFeO_x$ with Sub-Micrometer Spatial Resolution. *Adv. Func. Mater*. **2019**, 1901984.

22. Krebs H-U, Weisheit M, Faupel J, Süske E, Scharf T, Fuhse C, et al. Pulsed Laser Deposition (PLD) -- A Versatile Thin Film Technique BT - Advances in Solid State Physics. *Adv Solid State Phys*. **2003**, 43, 505-517.

23. Choi WK, Baek SY. Study on platinum coating depth in focused ion beam diamond cutting tool milling and methods for removing platinum layer. *Materials*. **2015**, 8(9), 6498–6507.

24. Rigort A, Plitzko JM. Cryo-focused-ion-beam applications in structural biology. *Arch Biochem Biophys.* **2015**, 581, 122–130.

25. Heinz WF, Hoh JH. Getting physical with your chemistry: Mechanically investigating local structure and properties of surfaces with the atomic force microscope. *J Chem Educ*. **2005**, 82(5), 695–703.

26. Shipp DW, Sinjab F, Notingher I. Raman spectroscopy: techniques and applications in the life sciences. *Adv Opt Photonics*. **2017**, 9(2), 315.

27. Ferreiro-Vila E, Bugallo D, Magén C, Rivadulla F, De Teresa JM. Topotactic transformation in $SrFeO_{3-\delta}$ triggered by low-dose Ga^+ focused ion irradiation. *Appl Phys Lett*. **2020**, 116(16), 163103.

28. Islam MA, Xie Y, Scafetta MD, May SJ, Spanier JE. Raman scattering in $La_{1-x}Sr_xFeO_{3-\delta}$ thin films: Annealing-induced reduction and phase transformation. *J Phys Condens Matter*. **2015**, 27(15), 155401.